

# A Time-Domain Inverse Dynamic Tracking Control of a Single-Link Flexible Manipulator<sup>1</sup>

**Dong-Soo Kwon**

Robotics & Process Systems Division,  
Oak Ridge National Laboratory,  
Oak Ridge, TN 37831-6304

**Wayne J. Book**

George W. Woodruff School  
of Mechanical Engineering,  
Georgia Institute of Technology,  
Atlanta, GA 30332

*A manipulator system with a large workspace volume and high payload capacity has greater link flexibility than do typical industrial robots and teleoperators. If link flexibility is significant, position control of the manipulator's end-effector exhibits nonminimum-phase, noncollocated, and flexible-structure system control problems. This paper addresses inverse dynamic trajectory planning issues of a single-link flexible manipulator. The inverse dynamic equation of a single-link flexible manipulator was solved in the time-domain. By dividing the inverse system equation into its causal part and anticausal part, the inverse dynamic method calculates the feed-forward torque and the trajectories of all state variables that do not excite structural vibrations for a given end-point trajectory. Through simulation and experiment with a single-link manipulator, the effectiveness of the inverse dynamic method in producing fast and vibration-free motion has been demonstrated.*

## 1 Introduction

A manipulator system with a large workspace volume and a large payload, such as the proposed long-reach manipulator for nuclear waste remediation or the Space Shuttle Manipulator Arm, has greater link flexibility than do typical industrial robots and teleoperators. If link flexibility is significant, control of the end-effector's position must cope with the nonminimum-phase, noncollocated, and flexible-structure control problems. The flexible manipulator system should be able to follow a given end-point trajectory to be used as a practical robotic manipulator in spite of its flexibility. This paper proposes an efficient time-domain inverse dynamic method that enables a flexible manipulator to follow a given end-point trajectory accurately without overshoot and residual vibration.

The regulating feedback control is one of the typical methods used to suppress the structural vibration of a manipulator. By using joint-and-strain feedback, Hastings and Book [1] demonstrated that structural vibration could be damped successfully. Even though the feedback control dampened the structural vibration, their experiments showed reverse action, overshoot, and flexible vibration to a step-position command. For a step-position command, these vibration phenomena are inevitable with the feedback control scheme because the feedback control signal contains high-frequency components that excite natural frequencies of the system. Instead of a step command, a smooth trajectory should be used as the end-point

reference command of a tracking control. However, the desired trajectories of flexible-mode variables are necessary to produce the desired output trajectories such as joint angle and strain. In the absence of realistic desired flexible-mode values, it has been common to assign a zero value to each desired flexible-mode variable to suppress vibration. In other words, joint commands are given to the flexible manipulator to follow the trajectory like a rigid manipulator. Even though the feedback tracking control reduces the vibration, such unrealistic commands are not always successful.

To avoid the aforementioned trajectory generation problem, De Luca and Siciliano [2] suggested a joint-based inversion control scheme. This method showed good tracking results for a certain joint trajectory, but it could not be extended to an end-point trajectory following control because of nonminimum-phase system characteristics. Oosting and Dickerson [3] proposed a calculation method for the torque to follow a smooth trajectory with a simple lumped-parameter model of a two-link flexible manipulator.

To make the end-point of a flexible manipulator follow a given trajectory, Bayo [4] proposed a new approach. For a given end-point acceleration profile, the required torque was calculated by solving the inverse dynamic equation in the frequency-domain with the inverse fast Fourier transform. Bayo pointed out that the inverse dynamic system, where the end-point acceleration is the input and the joint torque is the output, is a noncausal system because the output (torque) must begin before the input (end-point acceleration) begins. In spite of the excellent results reported, this method has a drawback. It requires extensive computation for the transformation of the dynamic model and the input trajectory from the time-domain to the frequency-domain. It also requires the inverse transformation of the output back to the time-domain. To reduce this computational burden, Bayo and Moulin [5] introduced

<sup>1</sup>Research sponsored by the National Aeronautics and Space Administration under grant no. NAG 1-623 in Georgia Institute of Technology, and preparation supported by the Office of Technology Development, U.S. Department of Energy, managed by Martin Marietta Energy Systems, Inc., under contract DE-AC05-84OR21400.

Contributed by the Dynamic Systems and Control Division for publication in the JOURNAL OF DYNAMIC SYSTEMS, MEASUREMENTS, AND CONTROL. Manuscript received by the DSCD November 1990; revised manuscript received January 5, 1993. Associate Technical Editor: R. Horowitz.

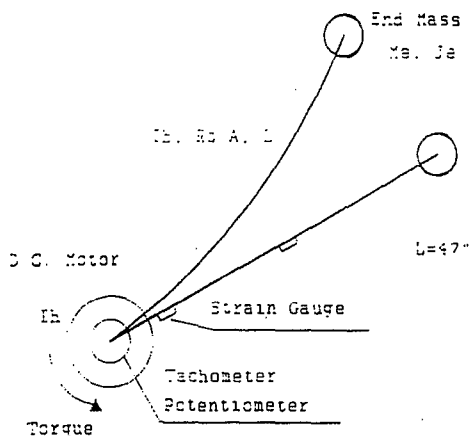


Fig. 1 A single-link flexible manipulator

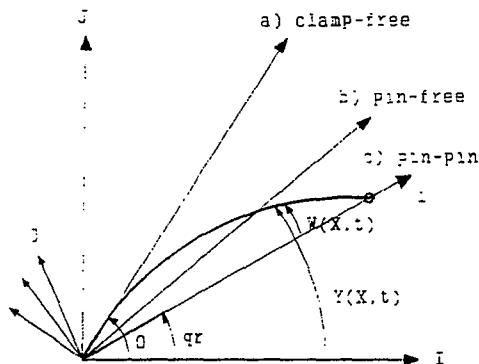


Fig. 2 The kinematic descriptions of flexible manipulator coordinates

the convolution integral method to solve the inverse dynamic equation.

Asada and Ma [6] derived an inverse dynamic equation by using assumed mode functions for a general  $n$ -link case. The transfer function of a flexible manipulator between the input (torque) and the output (end-point position) is nonminimum-phase, i.e., it has positive real zeros. These zeros become positive poles of the inverse dynamic system transfer function. The positive poles cause the inverse system to be unstable if the inverse system output is restricted to causal solutions. Asada and Ma showed nonlinear effects using rigid motion torque without solving the inverse dynamic equation completely.

Kwon and Book [7] introduced a new inverse dynamic method that considerably relieves the calculation burden. The required torque was calculated in the time-domain, and the desired trajectories of all states were obtained for a given end-point trajectory. These trajectories are used as the reference commands for feedback tracking control.

The generation of trajectories for all states considering flexible dynamics is one of the main advantages of this time-domain inverse dynamic method. The frequency-domain inverse dynamic method is based on the Fourier transform and its inverse with a single-input, single-output transfer function. Therefore, it provides only a torque corresponding to a desired end-point trajectory from one transfer function. The torque profile is used for feedforward open-loop control. To add a feedback loop, the joint-angle and strain trajectories considering the flexible dynamics are essential. The time-domain inverse dynamic method of this paper calculates the torque profile and desired reference trajectories including flexible coordinates for feedback tracking control from the same integration. As another advantage, this time-domain method can generate the torque profile for nonzero initial conditions (IC) and nonzero final conditions in the desired trajectory [8, 9].

In the frequency-domain method, the ICs are always assumed to be zeros. It is not easy to adapt to a nonzero IC trajectory.

This paper presents the time-domain inverse dynamic method with the detailed interpretation of this method in the frequency-domain. First, a single-link manipulator is described and modeled by using the assumed mode method. Second, the inverse dynamic equation is derived from the dynamic equation of the system in a state space form. Third, the time-domain inverse dynamic method is explained in the frequency-domain. Next, this inverse dynamic method is implemented through simulations on the single-link flexible manipulator. Results are compared with the output of other typical control methods. Finally, a tracking controller has been designed that combines the inverse dynamic feedforward control and the joint-feedback control, and its experimental results are presented and discussed.

## 2 Modeling

A single-link flexible manipulator having planar motion is described as shown in Fig. 1. The link is 47 in long; it is modeled with the rotational inertia,  $I_b$ , and the unit length mass,  $R_0 A$ . The rotating inertia of the servomotor, the tachometer, and the clamping hub are modeled as the hub inertia,  $I_h$ . The payload is modeled as the end mass,  $M_e$ , and the rotational inertia,  $J_e$ . Although structural damping exists in the flexible link, it is ignored in modeling.

To derive the equations of motion of the manipulator, we describe the position of a point on the beam with virtual rigid-body motion and deflection with respect to the rigid-body coordinate by using a Bernoulli-Euler beam model. The virtual rigid-body motion is represented by the motion of the moving coordinate attached to the beam. The deflection is described by a finite series of assumed modes.

In the assumed mode method, different mode shape functions have to be used depending on the choice of the rigid body coordinate. Several authors [1, 10] have used the rigid-body coordinate that is attached at the base ((a) of Fig. 2) with the clamped-free boundary condition mode functions. Other authors [11] defined the rigid-body coordinate to pass through the center of mass of the beam and used the pinned-free mode functions ((b) of Fig. 2). Others [6] let the rigid-body coordinate pass through the end-point and used the pinned-pinned mode functions ((c) of Fig. 2). All these definitions of the rigid-body coordinate are valid if appropriate mode functions satisfy the geometric boundary conditions. In this paper, the rigid-body mode coordinate that passes through the end-point of the beam is selected ((c) of Fig. 2), and the mode functions of pinned-pinned boundary conditions are used to describe the deflection of the beam.

To obtain an accurate model with a small number of modes, more accurate boundary conditions were considered reflecting the joint hub-inertia and the end-mass in addition to the geometric pinned-pinned boundary condition for the mode-shape functions. For the inverse dynamic model, the first two mode functions are used, and four modes are used for the manipulator plant model in simulation. Because of the selection of the rigid-body coordinate, the end-point position of the beam can be expressed by the rigid-body-mode variable alone. This simple representation of the end-point position allows easy derivation of the inverse dynamics equation.

By using Lagrange's equations of motion, the dynamic equation of a flexible manipulator is obtained with generalized coordinates. The detailed derivation is given in reference [7].

$$[M]\ddot{q} + [D]\dot{q} + [K]q = [B]r.$$

The dynamic equation can be divided into a rigid body part and a flexible part as follows:

$$\begin{bmatrix} M_{rr} & M_{rf} \\ M_{rf}^T & M_{ff} \end{bmatrix} \begin{Bmatrix} \ddot{q}_r \\ \ddot{q}_f \end{Bmatrix} + \begin{bmatrix} D_{rr} & D_{rf} \\ D_{rf}^T & D_{ff} \end{bmatrix} \begin{Bmatrix} \dot{q}_r \\ \dot{q}_f \end{Bmatrix} + \begin{bmatrix} 0 & 0 \\ 0 & K_{ff} \end{bmatrix} \begin{Bmatrix} q_r \\ q_f \end{Bmatrix} = \begin{bmatrix} B_r \\ B_f \end{bmatrix} \tau, \quad (1)$$

where

$q_r = q_0$  (rigid-body coordinate) and

$q_f = \begin{Bmatrix} q_1 \\ \vdots \end{Bmatrix}$  (flexible mode coordinate).

In the partitioned matrices, the subscript  $r$  denotes rigid and  $f$  denotes flexible; the mixture,  $rf$ , denotes coefficients of flexible coordinates in the rigid-body-mode equations.

For a state space form, we obtain the following dynamic Eq. (2). Hereafter, this dynamic equation is referred to as the direct dynamic equation to distinguish it from the inverse dynamic equation derived in Section 3.

$$\dot{X} = \begin{bmatrix} 0 & I \\ M^{-1}K & M^{-1}D \end{bmatrix} X + \begin{bmatrix} 0 \\ M^{-1}B \end{bmatrix} \tau; \quad (2)$$

$$Y = [C]X + [F]\tau,$$

where

$$\begin{aligned} X &= \{q_r, q_f, \dot{q}_r, \dot{q}_f\}^T \\ &= \{q_0, q_1, \dots, \dot{q}_0, \dot{q}_1, \dots\}^T. \end{aligned}$$

### 3 Inverse Dynamic Equations

From the direct dynamic equations, the inverse dynamic equation is derived, which represents the relationship between the desired acceleration of the rigid mode (equivalent to the tip acceleration) as input and the torque as output. Equation (1) can be written in two parts:

$$[M_{rr}]\ddot{q}_r + [M_{rf}]\ddot{q}_f + [D_{rr}]\dot{q}_r + [D_{rf}]\dot{q}_f = [B_r]\tau; \quad (3)$$

$$[M_{rf}]^T\ddot{q}_r + [M_{ff}]\ddot{q}_f + [D_{rf}]^T\dot{q}_r + [D_{ff}]\dot{q}_f + [K_{ff}]q_f = [B_f]\tau. \quad (4)$$

From Eq. (3), torque is expressed as

$$\tau = [B_r]^{-1} \{ [M_{rr}]\ddot{q}_r + [M_{rf}]\ddot{q}_f + [D_{rr}]\dot{q}_r + [D_{rf}]\dot{q}_f \}. \quad (5)$$

Substitution of Eq. (5) into Eq. (4) gives the following relations between the flexible coordinate  $q_f$  and the rigid body coordinate  $q_r$ .

$$[M_i]\ddot{q}_f + [D_i]\dot{q}_f + [K_i]q_f = [B_{i1}]\dot{q}_r + [B_{i2}]\ddot{q}_r, \quad (6)$$

where

$$[M_i] = \{ [M_{ff}] - [B_f][B_r]^{-1}[M_{rf}] \},$$

$$[D_i] = \{ [D_{ff}] - [B_f][B_r]^{-1}[D_{rf}] \},$$

$$[K_i] = [K_{ff}],$$

$$[B_{i1}] = \{ [B_f][B_r]^{-1}[D_{rr}] - [D_{rf}]^T \},$$

$$[B_{i2}] = \{ [B_f][B_r]^{-1}[M_{rr}] - [M_{rf}]^T \}.$$

From Eq. (4), the acceleration of the flexible coordinate is expressed as

$$\begin{aligned} \ddot{q}_f &= -[M_{ff}]^{-1}[M_{rf}]^T\ddot{q}_r - [M_{ff}]^{-1}[D_{rf}]^T\dot{q}_r \\ &\quad - [M_{ff}]^{-1}[D_{ff}]\dot{q}_f - [M_{ff}]^{-1}[K_{ff}]q_f + [M_{ff}]^{-1}[B_f]\tau. \end{aligned} \quad (7)$$

By substituting Eq. (7) into Eq. (3), we obtain

$$\tau = [C_{i1}]q_f + [C_{i2}]\dot{q}_f + [F_{i1}]\dot{q}_r + [F_{i2}]\ddot{q}_r, \quad (8)$$

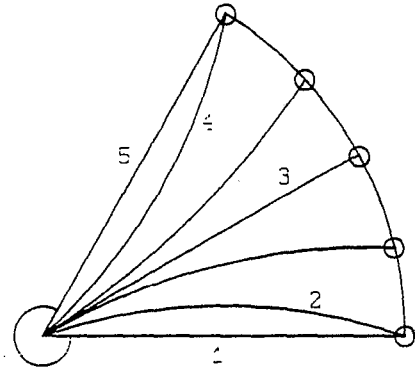


Fig. 3 Point-to-point motion of a flexible manipulator

where

$$[G] = \{ [B_r] - [M_{rf}][M_{ff}]^{-1}[B_f] \}^{-1},$$

$$[C_{i1}] = [G] \{ -[M_{rf}][M_{ff}]^{-1}[K_{ff}] \},$$

$$[C_{i2}] = [G] \{ [D_{rf}] - [M_{rf}][M_{ff}]^{-1}[D_{ff}] \},$$

$$[F_{i1}] = [G] \{ [D_{rr}] - [M_{rf}][M_{ff}]^{-1}[D_{rf}]^T \},$$

$$[F_{i2}] = [G] \{ [M_{rr}] - [M_{rf}][M_{ff}]^{-1}[M_{rf}]^T \}.$$

If Eqs. (6) and (8) are represented in a state space form, the inverse dynamic equations will be written in the following simple form. Let

$$X_i = \{q_f, \dot{q}_f\}^T \text{ and } q_{ir} = \{q_r, \dot{q}_r\}^T.$$

$$\dot{X}_i = \begin{bmatrix} 0 & I \\ M_i^{-1}K_i & M_i^{-1}D_i \end{bmatrix} X_i + \begin{bmatrix} 0 \\ M_i^{-1}B_{i1} & M_i^{-1}B_{i2} \end{bmatrix} \dot{q}_{ir},$$

$$\tau = [C_{i1}, C_{i2}]X_i + [F_{i1}, F_{i2}] \dot{q}_{ir};$$

$$\dot{X}_i = [A_i]X_i + [B_i]\dot{q}_{ir}$$

$$\tau = [C_i]X_i + [F_i]\dot{q}_{ir} \quad (9)$$

Since matrix  $A_i$  has positive real eigenvalues (which came from the positive zeros of the transfer function of the direct dynamic system) as well as negative real eigenvalues, integration of Eq. (9) will diverge in a causal sense. However, if the solution range of the equation is expanded to include noncausal solutions, a unique stable solution can be obtained by integrating this differential equation.

To analyze the inverse system to a flexible manipulator, let us define several terms. A causal system is a system in which the output (impulse response) always occurs after an input (impulse) is given. An anticausal system, however, always has the output (backward impulse response) before an input (impulse) is given. A noncausal system has the combined output of a causal system and an anticausal system. To grasp the meanings of the previous definitions, the physical phenomena of the actual motion of a flexible manipulator are described in Fig. 3. If a certain torque profile is applied to the manipulator, there is a unique motion of the end-point. On the other hand, if the same unique motion of the end-point is given as a desired motion, the same torque profile should be obtained by using the inverse dynamic equations. In most cases, to make the end-point follow a certain trajectory profile, we have to preshape (prebend) the flexible manipulator as shown by position 2 of Fig. 3. Therefore, the required torque, which is necessary to preshape it, must be applied from position 1 to 2 of Fig. 3 before the end-point starts to move. The torque (output of the inverse system) acts before the tip motion (input of the inverse system). This means that the inverse system has anticausal characteristics. When the flexible manipulator stops,

some torque should be applied to release the flexible deflection from position 4 to 5 of Fig. 3 after the end-point stops. This means that the inverse system has causal system characteristics, too. Thus, such an inverse system can be called a noncausal system, which is composed of a causal system and an anticausal system.

With this intuitive motivation, the inverse dynamic system can be divided into its causal and anticausal parts by using the following similarity transformation:

[ $T$ ]: similarity transformation matrix

$$X_i = [T]P_i = [T_c, T_{ac}] \{P_c, P_{ac}\}^T, \quad (10)$$

where  $X_i = \{q_r, \dot{q}_r\}^T$ . The  $T_c$ 's basis vectors are the eigenvectors that have negative eigenvalues, and  $T_{ac}$  is made of the eigenvectors of positive eigenvalues.

$$[T]^{-1}A_i[T] = \begin{bmatrix} A_{ic} & 0 \\ 0 & A_{iac} \end{bmatrix};$$

$$\begin{bmatrix} \dot{P}_c \\ \dot{P}_{ac} \end{bmatrix} = \begin{bmatrix} A_{ic} & 0 \\ 0 & A_{iac} \end{bmatrix} \begin{bmatrix} P_c \\ P_{ac} \end{bmatrix} + \begin{bmatrix} B_{ic} \\ B_{iac} \end{bmatrix} \dot{q}_{ir},$$

$$\begin{bmatrix} \tau_c \\ \tau_{ac} \end{bmatrix} = \begin{bmatrix} C_{ic} \\ C_{iac} \end{bmatrix} \begin{bmatrix} P_c \\ P_{ac} \end{bmatrix} + \begin{bmatrix} 1/2 F_i \\ 1/2 F_i \end{bmatrix} \dot{q}_{ir},$$

$$\tau = \tau_c + \tau_{ac}. \quad (11)$$

Such a coordinate change decouples the inverse system into two subsystems as shown in Eq. (11). The new variable  $P_c$  represents the coordinates of the causal system, and the  $P_{ac}$  represents that of the anticausal system. Even though [ $F_i$ ] is not required to be divided equally in causal and anticausal equations, it was divided equally to make the causal and anticausal systems' time-response symmetric.

For a given end-point trajectory, the causal part of the torque is obtained by integrating the causal part of the inverse dynamic equations forward in time, starting from the initial time of the trajectory. The anticausal system equations must be integrated backward in time, starting from the final time of the trajectory. The meanings of the forward and backward integrations are interpreted in detail in the frequency-domain in Section 4. The total torque, which is the output of Eq. (11), is obtained by adding the outputs of the causal and anticausal systems. In Section 6, Fig. 7 shows the calculated torque profiles for a certain desired trajectory.

As additional outputs of this inverse dynamic method, the reference trajectories of all flexible-mode coordinates have been calculated from the rigid-body-mode trajectory. As can be expected from Eqs. (2) and (11), the space of the full-state vector  $X$  of the direct dynamic system can be divided into three subspaces: the rigid-body coordinate subspace  $q_{ir}$ , the causal part flexible coordinate subspace  $P_c$ , and the anticausal part flexible coordinate subspace  $P_{ac}$ . These subspaces are linearly independent and orthogonal to each other. The relations of these spaces are illustrated in Fig. 4, and are described by Eq. (12), in which only two flexible modes are considered.

Where  $X = \{q_r, q_{f1}, q_{f2}, \dot{q}_r, \dot{q}_{f1}, \dot{q}_{f2}\}^T$ ,  $q_{ir} = \{q_r, \dot{q}_r\}^T$ , and  $X_i = \{q_{f1}, q_{f2}, \dot{q}_{f1}, \dot{q}_{f2}\}^T = [T]P_i$ ,

$$X = \begin{bmatrix} 1 & 0 \\ 0 & 0 \\ 0 & 0 \\ 0 & 1 \\ 0 & 0 \\ 0 & 0 \end{bmatrix} q_{ir} + \begin{bmatrix} 0 & 0 & 0 & 0 \\ 1 & 0 & 0 & 0 \\ 0 & 1 & 0 & 0 \\ 0 & 0 & 0 & 0 \\ 0 & 0 & 1 & 0 \\ 0 & 0 & 0 & 1 \end{bmatrix} X_i = H_r q_{ir} + H_f X_i$$

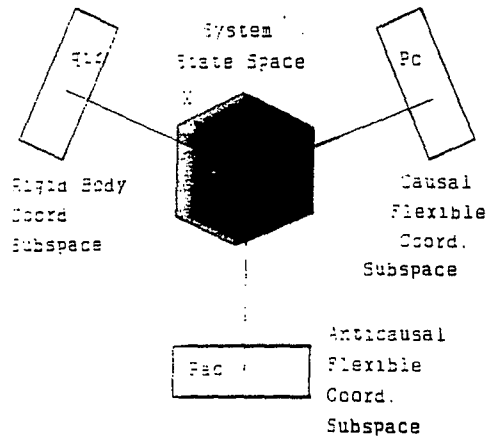


Fig. 4 Dimensional analysis of state variables of flexible-manipulator dynamic equations

$$= H_r q_{ir} + H_f [T]P_i = H_r q_{ir} + H_f T_c P_c + H_f T_{ac} P_{ac}. \quad (12)$$

From the given end-point trajectory, the rigid body coordinate trajectory  $q_{ir}$  is obtained. The flexible coordinate trajectories of  $P_c$  and  $P_{ac}$  are then calculated from the integration of Eq. (11). Then, the trajectories of all original states  $X$  can be obtained by Eq. (12). These trajectory values can be used as reference commands for feedback tracking control.

The generation of complete state trajectories is one substantial advantage of this time-domain inverse dynamic method over the other methods [2, 4, 12]. From the calculated state trajectories, the desired output trajectories can be obtained, such as joint angle, joint velocity, and strains as well as the inverse dynamic torque. Because the output trajectories were obtained considering the flexible dynamics, we no longer have to give reference commands for the flexible manipulator to follow the trajectory like a rigid manipulator by specifying that the desired strain be zero.

#### 4 Interpretation of the Inverse Dynamic Method in the Frequency-Domain

This section explains the separation of the inverse dynamic system into the causal and anticausal parts by using the two-sided Laplace transform and interprets the integration of causal and anticausal equations with the convolution integral. For simplicity, we will change the variable name  $\dot{q}_{ir}$  of the inverse dynamic Eq. (9) to  $q_a$ .

$$\dot{X}_i = [A_i]X_i + [B_i]q_a,$$

$$\tau = [C_i]X_i + [F_i]q_a. \quad (13)$$

Since the inverse system is noncausal,  $X_i(t)$  is nonzero for both  $t < t_f (=0)$  and  $t > t_f$ , while the end-point,  $q_a(t)$ , moves only for  $0 \leq t \leq t_f$ , the two-sided Laplace transform should be used to obtain the transfer function of the inverse system.

The two-sided Laplace transform  $L_2\{\}$  is defined over some strip of convergence as follows [13]:

$$X_i(s) = L_2\{X_i(t)\}$$

$$= \int_{-\infty}^{\infty} e^{-st} X_i(t) dt, \quad (14)$$

where  $\alpha < \text{Re}(s) < \beta$ .

Accordingly, the inverse two-sided Laplace transform is defined by

$$X_i(t) = L_2^{-1} \{X_i(s)\}$$

$$= \frac{1}{2\pi j} \int_{c-j\infty}^{c+j\infty} e^{st} X_i(s) ds \quad \text{for } \alpha < c < \beta. \quad (15)$$

The strip of convergence depends on the exponential convergence rate of the time response of the function  $X_i(t)$ .

Define the inverse system transfer function between the input (the rigid-body coordinate trajectory  $q_a$ ) and the output (the joint torque  $\tau$ ) as

$$H(s) = \frac{\tau(s)}{q_a(s)} \quad \text{for } \alpha < \text{Re}(s) < \beta. \quad (16)$$

Since  $H(s)$  has the same order denominator and numerator, it is separated into a strictly anticausal function  $H_1(s)$ , a strictly causal function  $H_2(s)$ , and a constant  $K$ . This constant ensures that  $H_1(s)$  and  $H_2(s)$  have a higher-order denominator than numerator to satisfy the condition of Jordan's Lemma [14].

$$H(s) = H_1(s) + H_2(s) + K. \quad (17)$$

Since the impulse response  $h(t)$  of the transfer function  $H(s)$  depends on the choice of the strip of convergence, the shaded region of Fig. 5 between the largest negative pole,  $a_1$ , and the smallest positive pole,  $b_1$ , has been chosen among several candidate strips of convergence such as  $\text{Re}(s) < a_2$ ,  $a_2 < \text{Re}(s) < a_1$ ,  $a_1 < \text{Re}(s) < b_1$ , . . . . Among them, only the shaded region provides a bounded stable time response for the inverse Laplace transform. Because the particular strip of convergence is chosen,  $H(s)$  is separated into  $H_1(s)$ , which has only positive poles corresponding to the eigenvalues of anticausal part system matrix  $A_{ac}$ , and  $H_2(s)$ , which has only negative poles corresponding to the eigenvalues of the causal part system matrix  $A_c$ . These explanations justify why the inverse system matrix  $A_i$  can be separated into  $A_{ac}$ , having only positive eigenvalues and  $A_c$ , having only negative eigenvalues.

The inverse Laplace transform of Eq. (17) is calculated along line AB in the strip  $a_1 < \text{Re}(s) < b_1$  [13]. Using the theorem on integration over large semicircles and Jordan's Lemma [14], the previous complex-plane contour integral along line AB of Fig. 5 is calculated as follows.

$$\text{For } t < 0, h(t) = \frac{1}{2\pi j} \oint_{ABCA} e^{st} H(s) ds$$

$$= \frac{1}{2\pi j} \int_{c-j\infty}^{c+j\infty} e^{st} H_1(s) ds + \delta(t)K$$

$$= -\Sigma \text{ residue of } e^{st} H_1(s) + \delta(t)K$$

$$= h_{ac}(t) + \delta(t)K. \quad (18)$$

$$\text{For } t > 0, h(t) = \frac{1}{2\pi j} \oint_{ABDA} e^{st} H(s) ds$$

$$= \frac{1}{2\pi j} \int_{c-j\infty}^{c+j\infty} e^{st} H_2(s) ds + \delta(t)K$$

$$= \Sigma \text{ residue of } e^{st} H_2(s) + \delta(t)K$$

$$= h_c(t) + \delta(t)K. \quad (19)$$

The inverse Laplace transform of Eq. (18) and Eq. (19) gives the impulse response function  $h(t)$ , which has an anticausal part,  $h_{ac}(t)$ , and a causal part,  $h_c(t)$ .

Next, the total torque calculation adding the causal part of

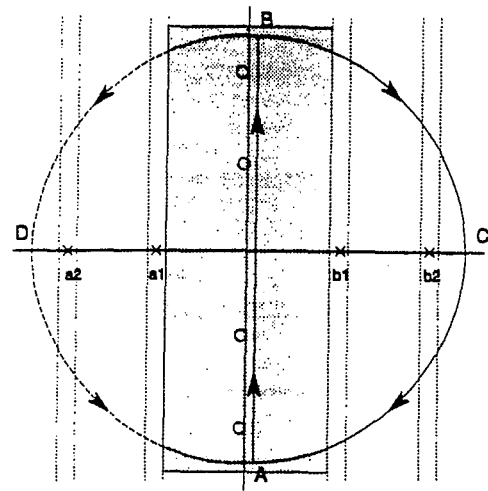


Fig. 5 Contour integrals in complex plane

the torque and the anticausal part of the torque will be interpreted with the convolution integral:

$$\tau(t) = L_2^{-1} \{H(s)q_a(s)\}$$

$$= \int_{-\infty}^{\infty} h(\eta)q_a(t-\eta)d\eta, \quad (20)$$

where  $q_a(t)$  is defined for  $0 \leq t \leq t_f$ , and 0 otherwise. Since  $h(t) = h_{ac}(t) + \delta(t)K$  for  $t \leq 0$ ;  $h_{ac}(t) = 0$  for  $t > 0$ , and since  $h(t) = h_c(t) + \delta(t)K$  for  $t \geq 0$ ;  $h_c(t) = 0$  for  $t < 0$ ,

$$\tau(t) = \int_{-\infty}^0 h_{ac}(\eta)q_a(t-\eta)d\eta + \int_0^{\infty} h_c(\eta)q_a(t-\eta)d\eta$$

$$+ \int_{-\infty}^{\infty} \delta(\eta)K q_a(t-\eta)d\eta$$

$$= \tau_{ac}^*(t \leq t_f) + \tau_c^*(t \geq 0) + K q_a(0 \leq t \leq t_f)$$

$$= \left\{ \tau_{ac}^*(t) + \frac{1}{2} K q_a(t) \right\} + \left\{ \tau_c^*(t) + \frac{1}{2} K q_a(t) \right\}$$

$$= \tau_{ac} + \tau_c, \quad (21)$$

where  $\tau_{ac}^* = 0$  for  $t > t_f$ ,  $\tau_{ac}^* = 0$  for  $t < 0$ ,  $q_a = 0$  for  $t < 0$  and  $t > t_f$ .

The torque Eq. (21) has the same form as Eq. (11). The convolution integral of  $\tau_{ac}^*$  is equivalent to the backward integration of the anticausal subsystem equation from  $t_f$  to  $-\infty$ ; the integral of  $\tau_c^*$  is the same as the integration of the causal subsystem equation from 0 to  $\infty$ . Thus, the total torque is composed of the anticausal part torque  $\tau_{ac}^*$ , the causal part torque  $\tau_c^*$ , and the input feedforward term  $Kq_a$ , which coincides with the term  $[F_i]q_a$  of the inverse dynamic equation.

## 5 Trajectory Generation

Theoretically, the inverse dynamic equation can give a torque profile for an arbitrary acceleration profile. However, as Bayo mentioned [12], it is important to apply an acceleration profile that does not excite the unmodeled dynamics of a manipulator. If the acceleration changes sharply, the calculated torque profile may excite the unmodeled high-frequency modes of the flexible manipulator. Furthermore, the torque frequency may be beyond the actuator bandwidth. The maximum acceleration limit also should be chosen properly to avoid saturation of the actuator and to use its full capacity for minimum traveling time. The minimum-traveling-time constraint makes the acceleration profile close to a bang-bang type, which will result in unwanted high-frequency problems. Therefore, the acceleration profile has to be selected by compromising the profile smoothness and the use of the full actuator capacity.

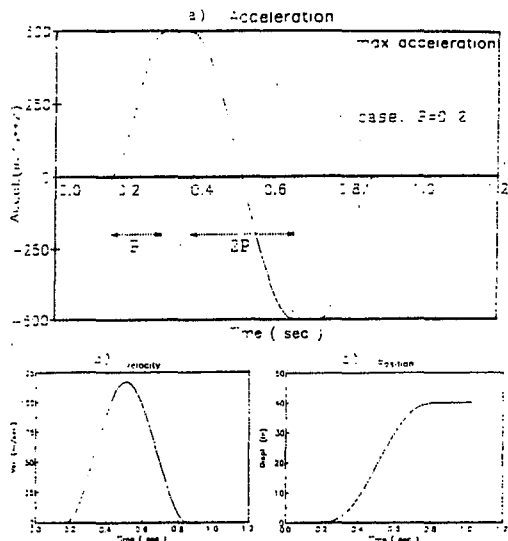


Fig. 6 Desired end point trajectory: (a) acceleration, (b) velocity, (c) position

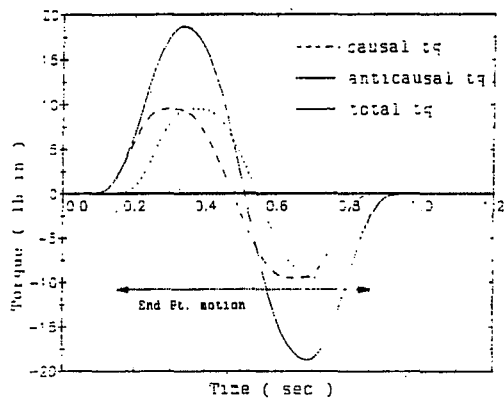


Fig. 7 Calculation of torque with the inverse dynamic method

Considering these trade-offs, the acceleration profile of Fig. 6 was used. It is composed of four third-order polynomial parts and two constant acceleration parts. The parameter  $P$  is the ratio of the first part polynomial acceleration time to the total traveling time of the end-point. If  $P=0$ , the profile will be the bang-bang type. If  $P=0.25$ , the profile will be very smooth because it is connected with four polynomials without constant acceleration parts. For simulations and experiments, the  $P=0.2$  case was used.

## 6 Simulation Results of the Inverse Dynamic Control

This section presents simulation results to illustrate the performance of the inverse dynamic method. First, the total torque profile is calculated from the causal part and the anticausal part of Eq. (11) for a given end-point acceleration profile, as shown in Fig. 7. The desired trajectories of the outputs such as joint angle, joint velocity, and strains are generated and are shown in Fig. 8. Theoretically, torque should be obtained by integrating to infinity. It is not clear how to determine the finite integral interval ( $t_s, t_f$ ) even though the time will depend dominantly on the inverse-system zeros closest to the origin and the input profile. In this paper, the torque profile was truncated at the time it dropped below 0.5 percent of the maximum torque value in order to apply the torque of the finite durations.

Second, the calculated torque was applied to the ideal flexible-manipulator model from which the inverse dynamic model

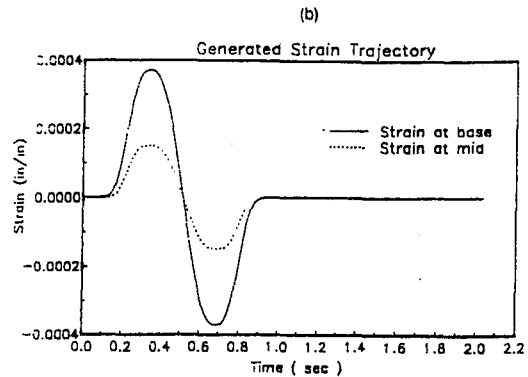
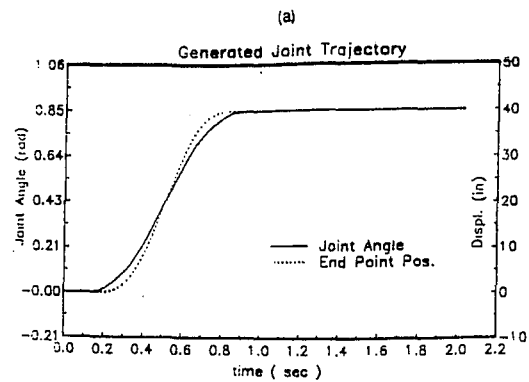


Fig. 8 Trajectory generation by using the inverse dynamic method: (a) joint angle, (b) strain at base, and at midpoint

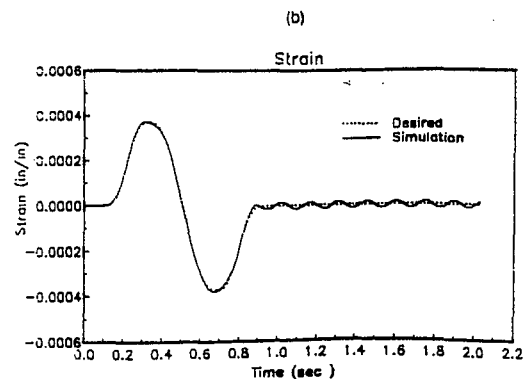
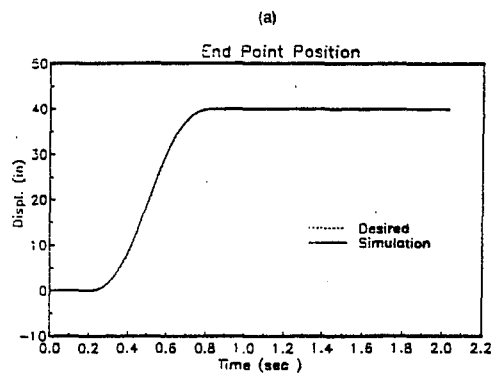


Fig. 9 Simulation of the open-loop control with the inverse dynamic method: (a) end-point position, (b) strain at base.

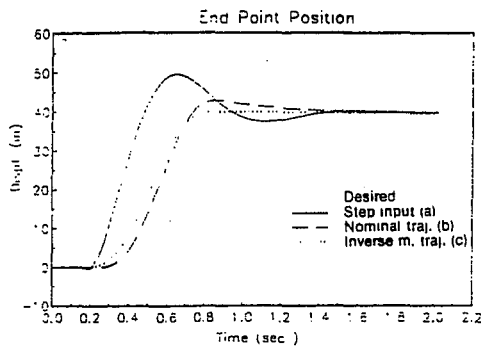


Fig. 10 Comparison of typical trajectories for feedback control methods: (a) step-input for joint feedback, (b) nominal trajectory for full-state feedback, and (c) inverse dynamic trajectory for full-state feedback.

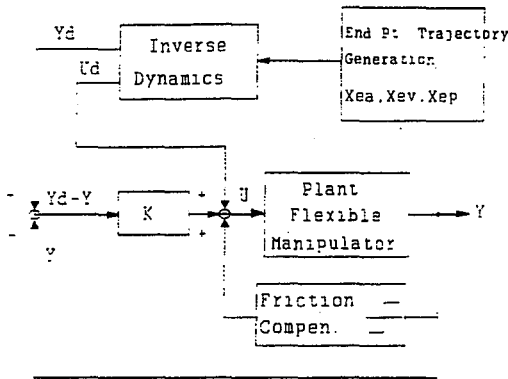


Fig. 11 Tracking control scheme of the experiment

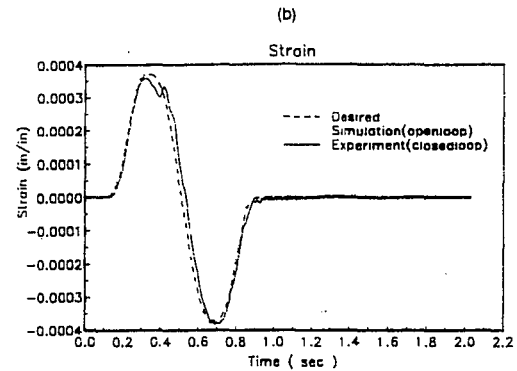
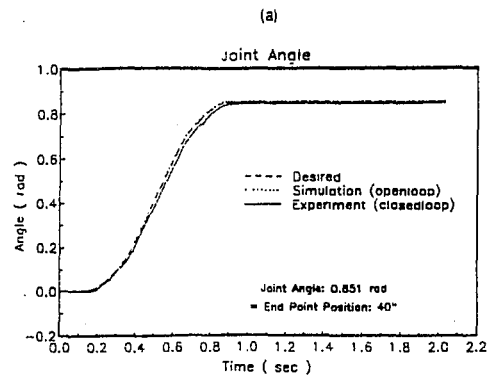


Fig. 12 Experimental results of the tracking control combined with the inverse dynamic feedforward control and the joint feedback control: (a) joint angle, (b) strain at the base

was derived. As shown in Fig. 9, the end-point follows the desired trajectory exactly, and no undershoot, overshoot, or noticeable residual vibration occur. However, the strain plot shows some residual oscillations after the end-point stops. These oscillations are caused by numerical integration errors that result from the somewhat slow sampling frequency (150 Hz) used in the simulation, which is the same as the sampling frequency of the experiment. When much higher sampling frequency was used, the residual vibration was almost unnoticeable.

Next, the effectiveness of inverse dynamic trajectories, which considered flexible dynamics, is demonstrated by comparing the simulation results of several typical feedback control methods. Figure 10 (curve a) is the result of a collocated joint P D controller for a step-input command. As can be expected, the feedback of position error generates very high peak torque at the beginning, and it excites the system's natural frequencies. Therefore, it requires a relatively long settling time. The result shows also the reverse action and the overshoot of the end-point position.

As an alternative method, a tracking full-state feedback controller was tried with a nominal joint trajectory. The nominal joint trajectory means that the trajectory is generated from the relation  $\theta = X_e/L$  between the joint and the end-point position based on rigid-link assumption. Consequently, the desired flexible coordinate values were set to zero:  $q_f = 0, \dot{q}_f = 0$ . The feedback gain was selected by the LQ method. Even though the response (curve b) is better than that of the step-input with joint feedback, it still has overshoot and requires a relatively long settling time. This poor tracking response is due to the unrealistic commands of zero values to the flexible coordinates. If compatible reference commands of the flexible modes are used, such as obtained from the inverse dynamic method, we can obtain good tracking performance. Figure 10 (curve c) shows almost no tracking error (and lies on top of the desired

response). This comparison clearly demonstrates the advantage of complete state trajectory generation by using the inverse dynamic method.

## 7 Experimental Results

Although the open-loop control with the inverse dynamic method showed good simulation results with an ideal model in Fig. 9, it produced a large positioning error with the experimental manipulator due to the effects of the joint friction. Therefore, a tracking controller was designed using the feedforward inverse dynamic method as shown in Fig. 11. A joint feedback control loop was added to provide robustness to the system, and a friction compensation loop was also added to cancel the effect of the friction force. If feedback gain of  $K(s)$  is very large, the joint-friction effect will be negligible, and the tracking performance will depend on the accuracy of the inverse system model [9]. Robustness issues with an inexact model are out of the scope of this paper, because the inverse dynamic method assumes the model's pole zero locations are accurate enough. However, the number of modes required for the inverse dynamic model depends on the desired trajectory frequency content. The inverse system model should have enough modes to filter out the frequency content of the desired trajectory, which may excite the structural vibration. For the proposed acceleration profile, a two-mode model was enough to be used as an inverse dynamic model. Comparative studies have been conducted using various orders in the inverse dynamic model [15]. Tracking error dynamics is analyzed for an inexact inverse model and disturbance in reference [9].

The combined tracking control scheme of the inverse dynamic feedforward control and the feedback control was implemented on the experimental single-link flexible manipulator. The manipulator used in the experiment is made of aluminum

beam (3/16×1×47-in.) and a 0.1-lb, end-mass. The natural frequencies of the experimental single link system are 6.6, 16.6, 41.8, and 81.9 Hz with a pinned-free boundary condition, including the hub-actuator rotational inertia and the end-mass. It is driven by an Inland dc servomotor with a current amplifier. For a real-time control, a Micro VAX II was used with 12-bit A/D and D/A boards. The off-line calculation of the trajectory and the torque profile was also performed by using the Micro VAX.

By applying the precalculated torque, compensating the joint friction, and using the feedback of the tracking error at the joint, the excellent results of Fig. 12 were obtained. The flexible manipulator could stop without any overshoot or any residual vibration after it moved 40 in. (48.76 deg) within less than 0.8 s. In the strain signal, a rough jerk exists that could be eliminated by using a smoother acceleration profile. Unfortunately, because the end-point position sensor was not available, the end-point position could not be measured directly. However, the end-point tracking performance can be estimated from the joint-tracking and the strain tracking result. If the joint does not have any overshoot or vibration and the strain does not show any residual vibration, the end-point can be presumed to stop without any overshoot or vibration.

In the experiment, only joint-angle and joint-velocity signals were used for feedback. The experimental results show that a simple joint feedback PD controller performs excellent tracking if it is combined with the inverse dynamic feedforward control and if the joint trajectories are provided considering the flexible dynamics. In the experimental system, the structural damping ratio was less than 0.02 for flexible vibration modes, and the hub joint has relatively large coulomb friction and proportional damping. The inverse dynamic method did not include the damping model. Only the joint friction has been compensated with the feedforward control based on the fiction model. The reasons why the results appear to show quite a bit of structural damping is that feedback control adds some active damping effect and the input torque did not excite structural vibration.

## 8 Conclusion

The proposed inverse dynamic method provides a simple way to generate the required torque profile and entire state trajectories in the time-domain for a flexible manipulator. In simulation, the use of the flexible coordinate trajectories generated by inverse dynamics resulted in much better feedback tracking performance than did nominal trajectory commands based on a rigid-link assumption. In laboratory experiments, feedforward control using the inverse dynamic method showed good tracking performance with a simple joint feedback controller. The measured outputs showed very small tracking er-

ror, no overshoot, and no oscillation, and they agreed well with the simulation results. The characteristics of the inverse dynamic system of a flexible manipulator were newly interpreted with the use of causal and anticausal concepts. Based on these concepts, the time-domain inverse dynamic method was interpreted in the frequency-domain in detail by using the two-sided Laplace transform in the frequency-domain and the convolution integral.

Although several successful results of this method are mentioned, this dynamic method is limited to linear systems. To be extended to a multilink flexible manipulator, this method should be incorporated with a nonlinear inversion technique, or use the dynamics of the manipulator linearized along the desired end-point trajectory.

## References

- Hasting, G., and Book, W. J., "Experiments in the Optimal Control of a Flexible Manipulator," *Proc. American Control Conference*, Boston, 1985, pp. 728-729.
- De Luca, A., and Siciliano, B., "Joint-Based Control of a Nonlinear Model of a Flexible Arm," *Proc. American Control Conference*, Atlanta, June 1988, pp. 935-940.
- Oosting, K., and Dickerson, S. L., "Simulation of a High-Speed Lightweight Arm," *Proc. of IEEE International Conference on Robotics and Automation*, Philadelphia, 1988, pp. 494-496.
- Bayo, E., "A Finite Element Approach to Control the End-Point Motion of a Single-Link Flexible Robot," *Journal of Robotic Systems*, Vol. 4, No. 1, pp. 63-75.
- Bayo, E., and Moulin, H., "An Efficient Computation of the Inverse Dynamics of Flexible Manipulators in the Time Domain," *Proc. IEEE Conference on Robotics and Automation*, 1989, pp. 710-715.
- Asada, H., and Ma, Z., "Inverse Dynamics of Flexible Robots," *Proceedings of the American Control Conference*, 1989, pp. 2352-2359.
- Kwon, D.-S., and Book, W. J., "An Inverse Dynamic Method Yielding Flexible Manipulator State Trajectories," *Proc. American Control Conference*, Vol. 1, San Diego, May, 1990, pp. 186-193.
- Book, W. J., and Kwon, D.-S., "Contact Control for Advanced Applications of Light Weight Arms," *Journal of Intelligent and Robotic Systems*, Vol. 6, 1992, pp. 121-137.
- Kwon, D.-S., and Book, W. J., "Tracking Control of a Nonminimum-Phase Flexible Manipulator," *Proc. ASME Winter Annual Meeting: Modeling and Control of Compliant and Rigid Motion Systems*, DSC-Vol. 31, 1991, pp. 27-37.
- Wang, D., and Vidyasagar, M., "Modelling and Control of Flexible Beam Using the Stable Factorization Approach," *Proc. ASME Winter Annual Meeting, Robotics: Theory and Application*, 1986, pp. 31-37.
- Cannon, R., and Schmitz, E., "Initial Experiments on End-Point Control of a Flexible One-Link Robot," *International Journal of Robotics Research*, Vol. 3, No. 3, 1984, pp. 49-54.
- Bayo, E., and Paden, B., "On Trajectory Generation for Flexible Robots," *Journal of Robotic Systems*, Vol. 4, No. 2, 1987, pp. 229-235.
- Pol, Balth, V. D., and Bremmer, H., *Operational Calculus Based on the Two-Sided Laplace Transform*, University Press at Cambridge, 1955.
- LePage, Wilbur, R., *Complex Variables and the Laplace Transform for Engineers*, McGraw-Hill, New York, NY 1961.
- Kwon, D.-S., *An Inverse Dynamic Tracking Control for Bracing a Flexible Manipulator*, Ph.D. dissertation, Georgia Institute of Technology, Atlanta, June 1991.